EXPLOITING NONLINEAR PROPERTIES OF VO_2 IN A MMWAVE ANTENNA-COUPLED SENSOR

Shangyi Chen[1], Mark Lust[2], and Nima Ghalichechian[3]*
[1]University of Pennsylvania, Philadelphia, Pennsylvania, USA
[2]The Ohio State University, Columbus, Ohio, USA
[3] Georgia Institute of Technology, Atlanta, Georgia, USA

ABSTRACT

We present the design, fabrication, and measurement of the antenna-coupled microbolometer using the phase change material vanadium dioxide (VO_2) for millimeter wave (mmWave) imaging applications. The nonlinear properties of VO_2 are exploited to achieve a large responsivity of 6.55×10^4 V/W by biasing the sensor through the metal-insulator transition (MIT) region. The overall performance of the sensor is also enhanced by suspending the device on the alumina (Al_2O_3) buffer layer membrane. The operating frequency band of the coplanar waveguide (CPW) fed dipole antenna is 31 – 55 GHz with on-wafer probe measurements. The radiation pattern of the 4×4 sensor array is demonstrated by the radar cross-section (RCS) technique using a highly precise robotic antenna measurement system.

KEYWORDS

Microbolometer, VO_2, antenna, millimeter wave, phase change material

INTRODUCTION

The bolometer is a sensor to quantify the radiation power through a material with a temperature dependent resistance. Since it was first introduced in 1880 [1], the bolometer has been widely used as a detector in a thermal camera for security screening, biomedical, and military applications. The functionality of the bolometer relies on the characteristic of the sensitive material's thermal coefficient of resistance (TCR). Electrical responsivity which is a chief figure of merit of the bolometer is directly proportional to TCR. Hence, one critical strategy to improve the responsivity of the bolometer is to utilize a material with a large TCR. Unfortunately, traditional microbolometers utilize linear materials that have small TCR (0.1%/K-0.3%/K), such as platinum [2], titanium [3], and bismuth [4].

Vanadium dioxide (VO_2) is an electrical phase change material that adopts insulating monoclinic (M1) phase (space group $P2_1/c$) below the transition temperature (~68 °C) and metallic tetragonal rutile (R) phase (space group $P4_2/mnm$) above the transition temperature [5-8]. Thus, VO_2 thin film whose electricity exhibiting a sharp change in the metal-insulator-transition (MIT) is appealing for a microbolometer to improve the responsivity. Especially, the TCR of VO_2 in the MIT region in our previous study can reach up to 171%/K [8, 9]. However, there are few studies demonstrating improved properties of microbolometer utilizing nonlinear properties of VO_2. For instance, VO_2 thin films have been utilized in the linear TCR region for infrared (IR) microbolometers as reported in [10]. Specifically, an eight-element uncooled VO_2 microbolometer linear array which exhibited a responsivity over 10 kV/W was described. While their proposed architecture was an on-substrate design, the reported large responsivity was mainly due to the large electrical resistivity of VO_2 thin films in the dielectric phase, which is unsuitable for the antenna coupling. The VO_2 microbolometer employing the phase-transition region and targeting for IR operation was described in [11]. The VO_2 microbolometer was biased on the semiconducting-metal phase transition with negative electrothermal feedback. Due to the on-substrate design and low quality of the deposited film with large hysteresis, only a small responsivity of 108 V/W with the ac bias technique was obtained.

Here, we employ VO_2 as the sensitive material to take the advantage of its large TCR in the MIT region to achieve high responsivity [12]. Our previous studies analytically demonstrated the approaches to enhance the responsivity of the microbolometer by the utilization of VO_2's nonlinearity in the MIT region and air suspension [9, 13, 14]. Also, the architecture of VO_2 thin film on alumina (Al_2O_3) buffer layer by the atomic layer (ALD) technique is adopted in this report to design and fabricate the sensor [8]. The VO_2 microbolometer is coupled with a dipole antenna and coplanar waveguide (CPW) designed to operate at 30 – 60 GHz. The CPW is used for excitation and biasing. The antenna transfers the electromagnetic power to VO_2 for sensor. The targeted millimeter wave (mmWave) band has obvious advantages over IR band, as mmWave is able to pass through opaque objects such as fog and clouds and can be used for imaging in harsh environments. To improve the thermal isolation as well as the antenna radiation efficiency, the VO_2 sensor is suspended on the Al_2O_3 buffer layer from the silicon (Si) substrate by the deep reactive ion etching (DRIE) process. Additionally, we utilize the 4×4 VO_2 microbolometer array to analyze the antenna radiation pattern as a proof of concept for future mmWave imaging camera.

MICROBOLOMETER DESIGN AND FABRICATION

To quantify the performance of the microbolometer, one figure of merit is the electrical responsivity, which is defined as

$$\Re = \frac{\Delta V}{\Delta P}. \quad (1)$$

ΔV is the change of the voltage output due the input power variance ΔP. The antenna is necessary to be employed in the microbolometer especially at the mmWave band to absorb the radiated power. The architecture of the proposed VO_2 microbolometer is demonstrated in Figure 1. The VO_2 microbolometer is coupled to a CPW-fed dipole antenna with a frequency range of 30 – 60 GHz. The dipole antenna (with a length of 4.4 mm and width of 1.5 mm) is designed to receive the radiated power at the mmWave band, resulting in a resistance change of the VO_2 sensitive material. The CPW feed structure is integrated for excitation and biasing. The dimension of the VO_2 sensor is 10 μm × 60 μm × 0.1 μm. The buffer layer Al_2O_3 is employed to provide a good basis for VO_2 property and mechanically support the sensor. The electrical resistivity contrast and maximum TCR in the MIT region of our fabricated VO_2 thin film on annealed Al_2O_3 buffer layer are 1.46×10^4 and 171%/K [8, 9]. In addition, the thermal isolation and antenna radiation are improved by releasing the senor from the Si substrate with a main cutout diameter of 5 mm and strategically placed ring structures.

The three-layer photolithography process is employed to fabricate the sensor as described in Figure 2. First, a 48-nm-thick Al_2O_3 is deposited on the 4-inch 300-μm-thick double-side polished Si substrate using the ALD process. The as-deposited Al_2O_3 buffer is annealed by the rapid thermal annealing (RTA) process to achieve

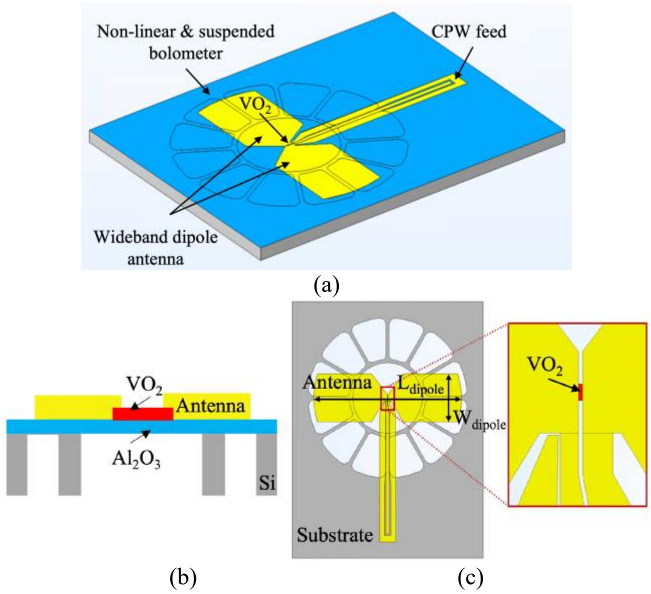

Figure 1: Antenna-coupled VO_2 microbolometer: (a)3D view, (b) cross-section view, and (c) top view.

the crystalline structure. The 100-nm-thick VO_2 thin film is then grown by reactive DC sputtering as detailed in [8], followed by a photolithography step. The VO_2 thin film is etched by the reactive ion etching (RIE) process for the sensor. The CPW-fed antenna is fabricated with a 250-nm-thick layer of gold using the e-beam evaporation and lift-off process. Finally, the device is released by etching the Si backside using the DRIE process.

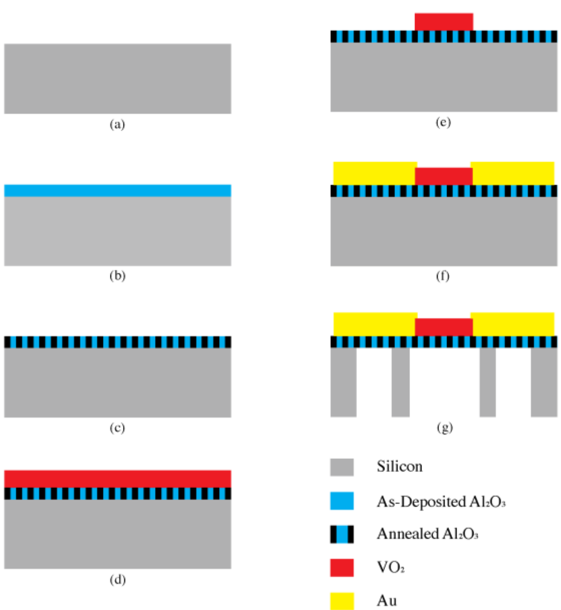

Figure 2: Fabrication process of antenna-coupled VO_2 microbolometer: (a) double-side polished Si, (b) ALD of Al_2O_3 buffer, (c) RTA of Al_2O_3 buffer, (d) sputtering of VO_2, (e) VO_2 RIE, (f) E-beam evaporation and lift off process for Au, and (g) Si backside DRIE.

MEASUREMENTS AND DISCUSSIONS

The antenna characterization, DC performance, and detection properties are carried out for the fabricated sensors.

Antenna Tests

The antenna tests include the impedance match analysis with the CPW-fed sensor and radiation measurements with the 4×4 sensor array. The CPW-fed sensor is measured on the probe station (Cascade M150) with a ground-signal-ground (GSG) 65 GHz probe (Infinity from FormFactor). A calibration standards substrate is used before mmWave measurements. The mmWave power is applied to the VO_2 microbolometer through the CPW by one port from the 67 GHz vector network analyzer (VNA). To excite the sensor, the DC electrical signal is applied with the same probe. A source meter (Keysight B2901A) is used to record the applied bias signals and the corresponding measured output signals. Figure 3 shows the on-wafer test setup and the arrangement of the probe with a detailed view of the probe on the sample. An external polyimide insulated heater (Omega Engineeing, Inc) is used under the sample to activate the sensor near the MIT region. A DC voltage of ~16.7 V is applied to the external heater using a power source (Keysight B2962A) and the surface temperature is measured to be ~59.4 °C by a thermocouple temperature probe. Figure 4 demonstrates the return loss (S_{11}) in frequencies ranging from 25 – 65 GHz measured by the VNA. VO_2 is at the dielectric phase without the DC voltage bias, and the antenna is not fully matched. With a DC voltage bias of 7 V that tunes the microbolometer through the MIT region, the frequency band ($S_{11} \leq$ -10 dB) increases, and the single element is matched from 31 – 55 GHz.

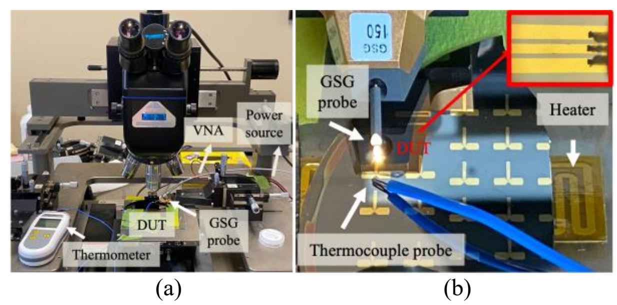

Figure 3: (a) The test setup for on-wafer measurement and (b) the detailed view of the probe on the sample.

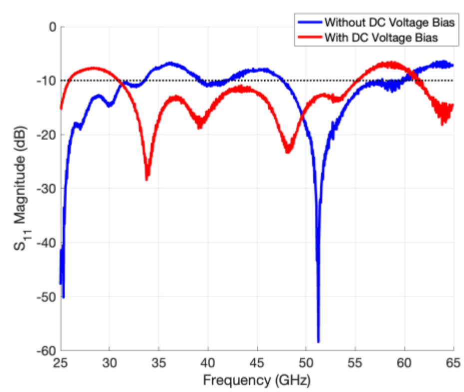

Figure 4: The S-parameter of the VO_2 microbolometer's antenna.

The gain pattern of the 4×4 VO_2 antenna-coupled microbolometer array operating at broadside is measured, as the antenna will only receive incoming radiation at narrow incidence angles in the full imaging system. We use the radar cross-section (RCS) technique which is a non-contact backscattering approach and featured to replace the cables and probs for the antenna gain measurement at the mmWave band [15]. As there is presently no read-out-circuit to control DC bias of the VO_2, the VO_2 resistors are in insulating state with a resistance of ~100 kΩ, giving high RF reflection ($S_{11} \approx 0$ dB). The VO_2 geometry in the array is adjusted from that in the CPW-fed sensor to be 10 µm × 200 µm. Therefore, in a full ROIC-controlled device, initial impedance of VO_2 can be set to ~75 Ω using temperature and DC voltage; this impedance will then fluctuate according to power level of incoming RF signal. As shown in Figure 5, we utilize a 6-axis robot system (Fanuc LR Mate200iD) developed in our previous study [16] with a dual-horn monostatic radar setup to measure radiation pattern. The standard gain horn antennas (QSH-SL-50-75-V-20) are used to establish signal floor by scanning the test setup without the microbolometer array in place. The 4×4 VO_2 microbolometer array is aligned with the horn antenna attached to the robot visually with a laser pointer, and a half-circle trajectory is carried out with a 0.33° angular resolution at a radius R=350mm from the end of the robot arm. The transmission coefficient (S_{21}) from the transmitting to the receiving horn antennas is obtained at 60 GHz during the trajectory. With constant distance, horn antenna gain, and wavelength, target gain factor varies only with excitation angle, so normalized antenna gain is proportional to S_{21}. Figure 6 shows normalized antenna array gain pattern with main lobe at 0° and side-lobes at ±20°, ±30°, and ±60° in E-plane and side lobes in H-plane, ranging from ±30° to ±60°. To account for the RCS contributions at the central angles from silicon, the measured curves in Figure 6 are adjusted by $n(2-\cos 2\theta)$, with n=2.5 in E plane and n=1.5 in H plane. In a fully realized imaging system, this antenna array design would successfully function at broadside. Although it has no need for receiving at the wider angles, they are beneficial for verifying simulated pattern.

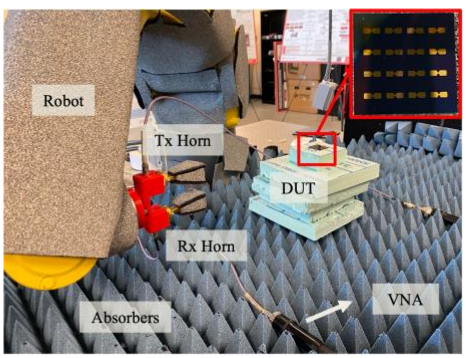

Figure 5: The test setup for RCS measurement.

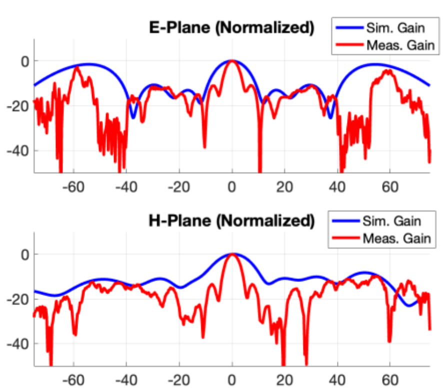

Figure 6: The normalized gain pattern of the 4×4 array.

DC/RF Characterization and Detection Properties

To excite the CPW-fed sensor through the MIT region, the DC bias and RF power are applied. The static I-V test of the CPW-fed VO_2 microbolometer is obtained as shown in Figure 7 when applying RF signal between 35 – 65 GHz controlled by the VNA. The RF power level ranges from -25 dBm – 0 dBm (3.1 µW – 1 mW). At each power level, the double-sweep voltage bias is applied, and the current is measured by the source meter. When the voltage bias increases, VO_2 starts from the linear dielectric phase, moves through the MIT region with a resistance of ~248 Ω where there is a sharp increase in the current, and enters the linear metallic region (~89 Ω resistance). As the voltage decreases, the hysteresis phenomenon is obvious and finally VO_2 moves back to the dielectric state. The required voltage triggering MIT decreases as the RF power increases as can be seen in Figure 7. The threshold voltage shift confirms that the microbolometer can sense the electromagnetic power change as low as -25 dBm (3.16 µW). The threshold voltage versus the input power is shown in Figure 8.

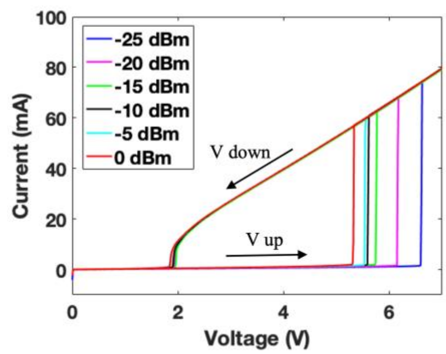

Figure 7: I-V curve of the VO_2 microbolometer.

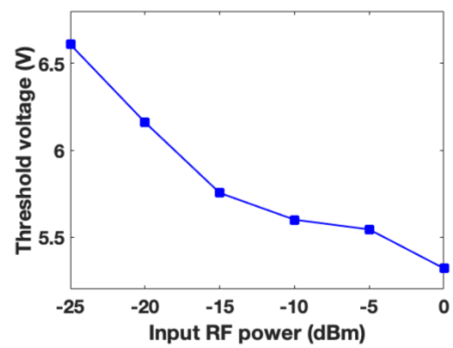

Figure 8: Threshold voltage versus input RF power.

The DC responsivity can be estimated from the ratio of the threshold voltage shift over the input power change to the VO_2 microbolometer, as defined in Eq. (1). The extracted DC responsivity versus corresponding RF power change is shown in Figure 9. Due to the nonlinear properties of VO_2 in the MIT region, the responsivity is highly nonlinear and has a larger value with a smaller RF power change. By the utilization of VO_2's large TCR in the MIT region and air suspension, our sensor can achieve a maximum DC responsivity of 6.55×10^4 V/W, which is $>10^2$ times larger than the state-of-the-art antenna-coupled microbolometers [17, 18] shown in Table 1.

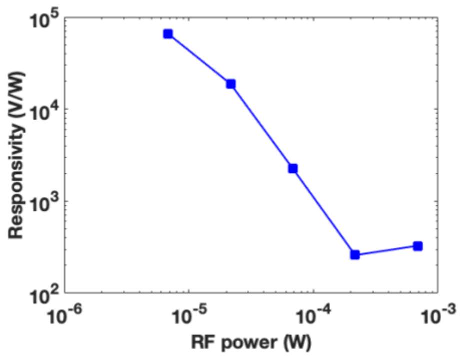

Figure 9: Responsivity versus RF power.

Table 1: Antenna-coupled microbolometer comparison.

	Specifications and performance		
	Material	Dimension (μm^3)	Responsivity (V/W)
This work	VO_2	10×60×0.1	6.55×10^4
[17]	Nb	10×1×0.35	85
[18]	$PrBa_2Cu_3O_{7-x}$	2×5×0.07	33

CONCLUSION

In this paper, the nonlinear properties of VO_2 thin films are exploited in the antenna-coupled microbolometer. The CPW-fed antenna operates in the frequency band of 31 – 55 GHz. For the proof of concept of an imager, the radiation pattern of the 4×4 sensor array is measured with the RCS technique. By biasing the sensor in the MIT region with the large TCR of VO_2 and using air suspension, our sensor demonstrates a high responsivity of 6.55×10^4 V/W. This work demonstrates the potential of employing VO_2 in a microbolometer to achieve a high responsivity for future mmWave imaging arrays.

ACKNOWLEDGEMENTS

This material is based upon work supported by the US National Science Foundation (NSF) CAREER Award under Grant No. 1845370 and 2149886, the Air Force Research Lab (AFRL)/Defense Associated Graduate Student Innovators (DAGSI) Award No. RY6-OSU-19-2-AFRL2, and AFOSR Lab Task 21RYCOR019 supported by Dr. Ilya Vitebskiy.

REFERENCES

[1] S. P. Langley, "The bolometer and radiant energy," *Proceedings of the American Academy of Arts and Sciences,* vol. 16, pp. 342-358, 1880.

[2] S. Yoneoka *et al.*, "ALD-metal uncooled bolometer," in *2011 IEEE 24th International Conference on Micro Electro Mechanical Systems*, 2011, pp. 676-679.

[3] A. Tiwari, H. Satoh, M. Aoki, M. Takeda, N. Hiromoto, and H. Inokawa, "Fabrication and analytical modeling of integrated heater and thermistor for antenna-coupled bolometers," *Sensors and Actuators A: Physical,* vol. 222, pp. 160-166, 2015.

[4] D. Neikirk, W. W. Lam, and D. Rutledge, "Far-infrared microbolometer detectors," *International journal of infrared and millimeter waves,* vol. 5, no. 3, pp. 245-278, 1984.

[5] J. B. Goodenough, "The two components of the crystallographic transition in VO2," *Journal of Solid State Chemistry,* vol. 3, no. 4, pp. 490-500, 1971.

[6] K. Liu, S. Lee, S. Yang, O. Delaire, and J. Wu, "Recent progresses on physics and applications of vanadium dioxide," *Materials Today,* vol. 21, no. 8, pp. 875-896, 2018.

[7] R. Shi *et al.*, "Recent advances in fabrication strategies, phase transition modulation, and advanced applications of vanadium dioxide," *Applied Physics Reviews,* vol. 6, no. 1, p. 011312, 2019.

[8] M. Lust, S. Chen, C. E. Wilson, J. Argo, V. Doan-Nguyen, and N. Ghalichechian, "High-contrast, highly textured VO2 thin films integrated on silicon substrates using annealed Al2O3 buffer layers," *Journal of Applied Physics,* vol. 127, no. 20, p. 205303, 2020.

[9] S. Chen, M. Lust, and N. Ghalichechian, "Multiphysics simulation of hypersensitive microbolometer sensor using vanadium dioxide and air suspension for millimeter wave imaging," *Microsystem Technologies,* vol. 27, no. 7, pp. 2815-2822, 2021.

[10] C. Chen, X. Yi, X. Zhao, and B. Xiong, "Characterizations of VO2-based uncooled microbolometer linear array," *Sensors and Actuators A: Physical,* vol. 90, no. 3, pp. 212-214, 2001.

[11] C. D. Reintsema, E. N. Grossman, and J. A. Koch, "Improved VO2 microbolometers for infrared imaging: operation on the semiconducting-metallic phase transition with negative electrothermal feedback," in *Infrared Technology and Applications XXV*, 1999, vol. 3698, pp. 190-201: International Society for Optics and Photonics.

[12] S. Chen, M. Lust, and N. Ghalichechian, "Antenna-coupled VO2 microbolometer for mmWave sensing," *IEEE Sensors Journal,* (under review).

[13] S. Chen, B. Ghassemiparvin, and N. Ghalichechian, "The design of high-responsivity millimeter wave imager using vanadium dioxide microbolometers," in *12th European Conference on Antennas and Propagation*, 2018, pp. 1-4.

[14] S. Chen, M. Lust, and N. Ghalichechian, "A vanadium dioxide microbolometer in the transition region for millimeter wave imaging," in *2019 IEEE International Symposium on Antennas and Propagation and USNC-URSI Radio Science Meeting*, 2019, pp. 1641-1642.

[15] J. Li, C. Matos, S. Chen, and N. Ghalichechian, "Fundamental improvement to the efficiency of on-chip mmWave phased arrays using MEMS suspension," *IEEE Antennas and Wireless Propagation Letters,* vol. 20, no. 4, pp. 473-477, 2021.

[16] C. Matos, J. Humanchuk, and N. Ghalichechian, "Robotically-controlled antenna measurement system for millimeter-wave applications," *Microwave and Optical Technology Letters,* vol. 63, no. 5, pp. 1520-1525, 2021.

[17] A. J. Miller, A. Luukanen, and E. N. Grossman, "Micromachined antenna-coupled uncooled microbolometers for terahertz imaging arrays," in *Terahertz for Military and Security Applications II*, Orlando, FL, 2004, vol. 5411, pp. 18-24.

[18] A. Scheuring *et al.*, "Thin Pr–Ba–Cu–O film antenna-coupled THz bolometers for room temperature operation," *IEEE Transactions on Terahertz Science and Technology,* vol. 3, no. 1, pp. 103-109, 2013.

CONTACT

*N. Ghalichechian, tel: +1-404-894-5867; nima.1@gatech.edu